URSI GASS 2020, Rome, Italy, 29 August - 5 September 2020

Characteristic Modes Extraction of Dielectric Bodies Using Pulse Functions

Sevda Özdemir*(1), Shang Xiang(2), and Buon Kiong Lau(2)
(1) Department of Electrical and Electronics Engineering, Hacettepe University, Ankara, Turkey
(2) Electrical and Information Technology, Lund University, Lund, Sweden

Abstract

This paper focuses on the use of pulse functions and point matching method to construct the impedance matrix needed for the characteristic mode analysis of dielectric bodies. Taking the results given by a commercial Method of Moments (MoM) solver as a benchmark, the proposed method is shown to facilitate accurate characteristic eigenvectors and eigenvalues on these structures using low order basis functions. The accuracy and feasibility of the proposed method are demonstrated in the numerical examples.

1 Introduction

Initiated by Garbacz [1] and refined by Harrington and Mautz [2], Characteristic Mode Analysis (CMA) has become increasingly popular for antenna design and optimization over the last decade. CMA is capable of characterizing an arbitrary object's radiation and scattering properties, relying only on its geometry and material properties, rather than the source configuration. This feature makes it an attractive candidate for formulating systematic design methods to handle complicated functionality trade-offs. CMA for structures with dielectric materials can be solved using Surface Integral Equation (SIE) and Volume Integral Equation (VIE) [3]-[4]. Though VIE is disadvantageous due of high mesh density and central processing unit (CPU) time, it does not suffer from spurious modes as SIE (when SIE is forced symmetric), and it does not require any additional computation to get the inner field data. Another advantage of VIE is that it can treat highly inhomogeneous structures like metamaterials without increasing the mesh density.

This paper proposes the computation of the characteristic modes (CMs) of dielectric objects using low-order basis functions (pulse functions) in VIE which to the authors' knowledge has not been done before. This method is chosen for its simplicity, relatively small error in calculating of the electric current volume integral equation (J-VIE) [5], and the ease of obtaining of geometry information. In Section 2, the theory of VIE and the theory of CMs is presented. In Section 3, the CMs obtained using pulse functions are compared to those obtained using Schaubert-Wilton-Glisson (SWG) basis functions in Altair FEKO® (Version 2018). Finally, some concluding remarks and possible future work will be given.

2 Theory

In Figure 1, an electromagnetic (EM) scattering problem is shown with incident plane wave $\boldsymbol{E}^i$ and $\boldsymbol{H}^i$ illuminating a three-dimensional inhomogeneous body with volume V, and material parameters (ε_d, μ_d). By utilizing volume equivalence principle (VEP), the EM scattering problem can be formulated in terms of equivalent volume electric current $\boldsymbol{J}(\boldsymbol{r})$ and equivalent volume magnetic current $\boldsymbol{M}(\boldsymbol{r})$. The formulation will be provided in the next section.

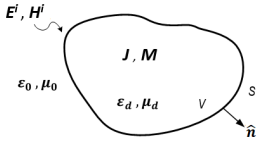

Figure 1. Scattering problem from a 3-D inhomogeneous object illuminated by the sources $\boldsymbol{E}^i$ and $\boldsymbol{H}^i$.

2.1 Derivation of VIE Using Pulse Functions

The electric field integral equation (EFIE) is written in terms of the electric current density $\boldsymbol{J}(\boldsymbol{r})$ for an inhomogeneous isotropic dielectric body ($\varepsilon_d \neq 1$, $\mu_d = 1$) as [6]

$$\boldsymbol{E}(\boldsymbol{r}) = \boldsymbol{E}^i(\boldsymbol{r}) + \boldsymbol{E}^s(\boldsymbol{r}), \tag{1}$$

where $\boldsymbol{E}(\boldsymbol{r})$ is the total electric field, $\boldsymbol{E}^i(\boldsymbol{r})$ the incident electric field and $\boldsymbol{E}^s(\boldsymbol{r})$ the scattered electric field. $\boldsymbol{E}^s(\boldsymbol{r})$ is defined as

$$\boldsymbol{E}^s(\boldsymbol{r}) = -\frac{j\omega\mu_0}{4\pi}\int_{V'}\boldsymbol{J}(\boldsymbol{r}')G dv' - \frac{\nabla}{j\omega 4\pi\varepsilon_0}\oint_{S'}\hat{\boldsymbol{n}}\cdot\boldsymbol{J}(\boldsymbol{r}')G ds'. \tag{2}$$

Here, $G = exp(-jkR)/R$ is the Green's function, R is the distance between source and field points and $\hat{\boldsymbol{n}}$ is unit outward unit vector normal to the surface of the dielectric. For numerical computation purposes, the dielectric region is divided into tetrahedral cells and the electric current density is expanded using pulse functions as

$$\boldsymbol{J}(\boldsymbol{r}) = \sum_{i=1}^{M}(\hat{\boldsymbol{x}}J_i^x\mathscr{P}_i(\boldsymbol{r}) + \hat{\boldsymbol{y}}J_i^y\mathscr{P}_i(\boldsymbol{r}) + \hat{\boldsymbol{z}}J_i^z\mathscr{P}_i(\boldsymbol{r})), \tag{3}$$

where M is the number of tetrahedron, J_i^x, J_i^y and J_i^z denote the x, y, z components of electric current density, respectively. $\mathscr{P}_i(\boldsymbol{r})$ represents the pulse basis function defined in

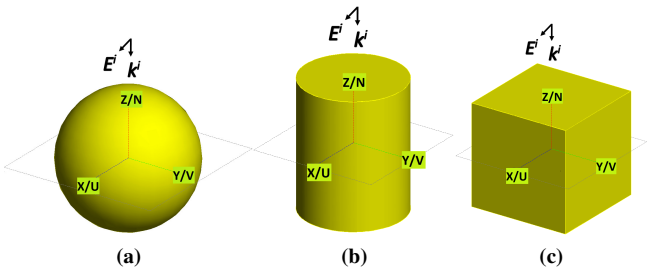

Figure 2. Geometry of the problems with the incident angles $\theta = 0^\circ$, $\phi = 0^\circ$ and $f_0 = 1$ GHz, a) Problem 1, a sphere of radius $r = 0.2\lambda_0$, b) Problem 2, a cylinder of radius $r = 0.1\lambda_0$ and height $h = 0.25\lambda_0$, c) Problem 3, a cube of side length $\ell = 0.2\lambda_0$.

the volume elements. After applying the point matching technique, the linear equations obtained for the unknown current density $\boldsymbol{J}(\boldsymbol{r}) = \hat{\boldsymbol{x}}J_x + \hat{\boldsymbol{y}}J_y + \hat{\boldsymbol{z}}J_z$ are derived as

$$\begin{bmatrix} Z(\boldsymbol{J}_{ij}^{xx}) & Z(\boldsymbol{J}_{ij}^{xy}) & Z(\boldsymbol{J}_{ij}^{xz}) \\ Z(\boldsymbol{J}_{ij}^{yx}) & Z(\boldsymbol{J}_{ij}^{yy}) & Z(\boldsymbol{J}_{ij}^{yz}) \\ Z(\boldsymbol{J}_{ij}^{zx}) & Z(\boldsymbol{J}_{ij}^{zy}) & Z(\boldsymbol{J}_{ij}^{zz}) \end{bmatrix} \begin{bmatrix} J_x \\ J_y \\ J_z \end{bmatrix} = \begin{bmatrix} E_x^{inc} \\ E_y^{inc} \\ E_z^{inc} \end{bmatrix}. \quad (4)$$

2.2 TCM on MoM

As suggested by Harrington, et al. [3], the TCM for an arbitrarily shaped dielectric object is formulated on top of EFIE due to impressed current $\boldsymbol{J}$ as follows

$$Z_V(\boldsymbol{J}) + (j\omega\Delta\varepsilon)^{-1}\boldsymbol{J} = \boldsymbol{E}^i, \quad (5)$$

where $\Delta\varepsilon = \varepsilon - \varepsilon_0$. After introducing the impedance operator $Z = Z_V + (j\omega\Delta\varepsilon)^{-1}$, (5) can be written as

$$Z(\boldsymbol{J}) = \boldsymbol{E}^i. \quad (6)$$

The eigenvalue equation using TCM is defined as follows

$$X \cdot \boldsymbol{J}_n = \lambda_n R \cdot \boldsymbol{J}_n, \quad (7)$$

where the real and imaginary parts of the EFIE impedance operator Z are denoted as R and X, respectively. All λ_n and $\boldsymbol{J}_n$ correspond to the characteristic values and currents of the generalized eigenvalue problem are real-valued. The characteristic currents $\boldsymbol{J}_n$ hold the following orthogonality relationships

$$\begin{aligned} \langle \boldsymbol{J}_m^*, R\boldsymbol{J}_n \rangle &= \langle \boldsymbol{J}_m, R\boldsymbol{J}_n \rangle = \delta_{mn} \\ \langle \boldsymbol{J}_m^*, X\boldsymbol{J}_n \rangle &= \langle \boldsymbol{J}_m, X\boldsymbol{J}_n \rangle = \lambda_{mn}\delta_{mn} \\ \langle \boldsymbol{J}_m^*, Z\boldsymbol{J}_n \rangle &= \langle \boldsymbol{J}_m, Z\boldsymbol{J}_n \rangle = (1+\lambda_{mn})\delta_{mn}, \end{aligned} \quad (8)$$

where δ_{mn} is Kronocker delta (0 if $m \neq n$, and 1 if $m = n$). Further, under external excitations, the induced current can be defined with the combination of all the modal solutions on an object [2] as

$$\boldsymbol{J} = \sum_{n=1}^{M} \frac{V_n^i \boldsymbol{J}_n}{1 + j\lambda_n}, \quad (9)$$

where the modal weighting coefficient V_n^i is

$$V_n^i = \langle \boldsymbol{J}_n, \boldsymbol{E}^i \rangle = \int_{V'} \boldsymbol{J}_n \cdot \boldsymbol{E}^i d\tau'. \quad (10)$$

The complex power radiated by the induced current $\boldsymbol{J}$ in the dielectric body illuminated by the incident field $\boldsymbol{E}^i$ is given by

$$P = \langle \boldsymbol{J}^*, Z\boldsymbol{J} \rangle = \langle \boldsymbol{J}^*, R\boldsymbol{J} \rangle + j\langle \boldsymbol{J}^*, X\boldsymbol{J} \rangle. \quad (11)$$

For the n-th CM, the real part of $\langle \boldsymbol{J}_n^*, Z\boldsymbol{J}_n \rangle$, which is radiated power, and the imaginary part of $\langle \boldsymbol{J}_n^*, Z\boldsymbol{J}_n \rangle$, are given below, respectively.

$$\begin{aligned} \langle \boldsymbol{J}_n^*, R\boldsymbol{J}_n \rangle &= Re\langle \boldsymbol{J}_n^*, Z\boldsymbol{J}_n \rangle = Re(P) \\ \langle \boldsymbol{J}_n^*, X\boldsymbol{J}_n \rangle &= Im\langle \boldsymbol{J}_n^*, Z\boldsymbol{J}_n \rangle - \tfrac{1}{\omega}\int_{V'} \boldsymbol{J}_n^* \cdot (\Delta\varepsilon)^{-1}\boldsymbol{J}_n dv'. \end{aligned} \quad (12)$$

3 Numerical Examples and Results

The three electromagnetic scattering problems depicted in Figure 2 were solved by VIE-MoM solution utilizing pulse basis functions and point matching built in Matlab®. The results were compared with those obtained with Altair FEKO® (Version 2018) which uses SWG basis functions for the solution of VIE [7]. The scatterers under investigation were discretized into tetrahedrons using the frequency $f_0 = 1$ GHz and wavelength $\lambda_0 = c/f_0$, c is the speed of light. The mesh information was extracted from Altair FEKO® and FEMLAB®. The incident angles of the plane wave were $\theta^i = 0^\circ$ and $\phi^i = 0^\circ$, where θ and ϕ are spherical coordinate angles. The power ratios (PRs) of the real and imaginary parts of $\langle \boldsymbol{J}^*, Z\boldsymbol{J} \rangle$ for the proposed (pulse) and SWG methods can be calculated as follows

$$PR_{real} = \frac{Re\langle \boldsymbol{J}^*, Z\boldsymbol{J} \rangle_{pulse}}{Re\langle \boldsymbol{J}^*, Z\boldsymbol{J} \rangle_{SWG}}, \quad PR_{imag} = \frac{Im\langle \boldsymbol{J}^*, Z\boldsymbol{J} \rangle_{pulse}}{Im\langle \boldsymbol{J}^*, Z\boldsymbol{J} \rangle_{SWG}}. \quad (13)$$

A convergence study of $\boldsymbol{J}$ was performed using the error norm between CMA calculated by (9) for the proposed and SWG methods, as defined by

$$Error(\boldsymbol{J}) = \frac{\|\boldsymbol{J}_{pulse} - \boldsymbol{J}_{SWG}\|}{\|\boldsymbol{J}_{SWG}\|}. \quad (14)$$

In the first example (sphere of radius 0.2 λ_0), five different mesh densities obtained from Altair FEKO® and FEMLAB® are illustrated in Figure 3, to compare the effect of number of meshes and different mesh types on CMA. For this analysis, the tetrahedron edge lengths (TELs) were chosen as $\lambda_{eff}/5$, $\lambda_{eff}/7.5$, and $\lambda_{eff}/10$, for meshing with Altair FEKO®, resulting in 307, 1160, and 2772 tetrahedrons, respectively ($\lambda_{eff} = \lambda_0/\sqrt{\varepsilon_r}$). For meshing with FEMLAB®, TELs of $\lambda_{eff}/5$ and $\lambda_{eff}/10$ were chosen, resulting in 302 and 3398 tetrahedrons, respectively. The results are compared using the CM results of Altair FEKO® for 307, 1160, 2772, 307, and 2772 tetrahedrons, respectively. As can be seen in Figure 3, as the number of meshes

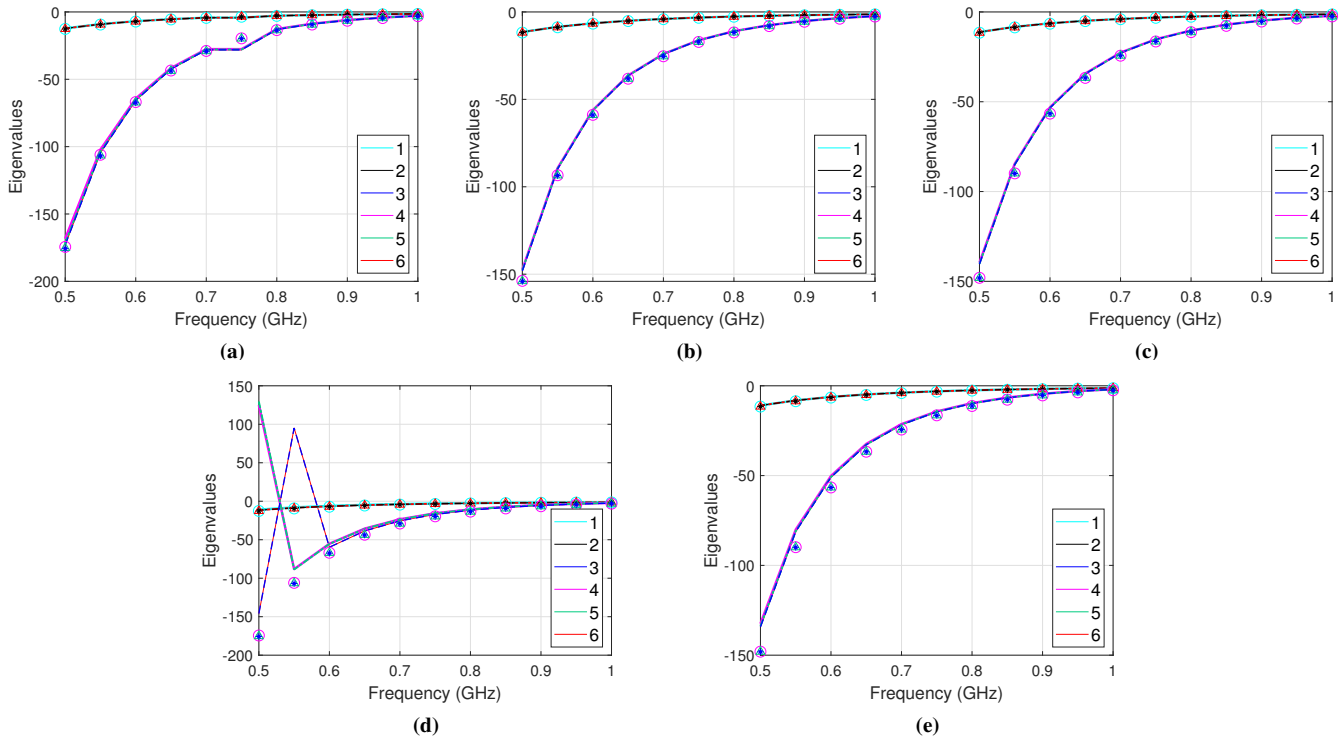

Figure 3. Eigenvalues of the first 6 CMs of a $0.2\lambda_0$ sphere for different number of meshes, $\varepsilon_r = 4$ (The coloured shapes $\circ$, $\triangle$, $*$ are for FEKO®'s CM results), (a) TEL=$\lambda_{eff}/5$, 307 tetrahedrons, (b) TEL=$\lambda_{eff}/7.5$, 1160 tetrahedrons, (c) TEL=$\lambda_{eff}/10$, 2772 tetrahedrons, (d) TEL=$\lambda_{eff}/5$, 302 tetrahedrons, (e) TEL=$\lambda_{eff}/10$, 3398 tetrahedrons.

increases, the characteristic eigenvalues appear to converge well for the first 6 CMs when the TEL is $\lambda_{eff}/10$. The first three degenerate CMs of the sphere have nearly the same eigenvalue, with a sufficiently large number of meshes, as can be seen in Table 1. This is also the case for the next three degenerate CMs (see Table 1), different meshes generated by Altair FEKO® and FEMLAB® change the CM results, especially for the larger (negative) eigenvalues, showing that different meshes can lead to some differences in the calculated eigenvalues of non-significant modes.

Table 1. The eigenvalue of first 6 thw CMs for the $0.2\lambda_0$ sphere for different number of meshes at $f_0 = 1$ GHz (meshing with Altair FEKO®, solved using pulse functions).

CM #	$\lambda_{eff}/5$	$\lambda_{eff}/10$	$\lambda_{eff}/12.5$
1	-1.330	-1.293	-1.291
2	-1.332	-1.297	-1.293
3	-1.337	-1.299	-1.295
4	-2.355	-2.142	-2.128
5	-2.370	-2.167	-2.139
6	-2.388	-2.172	-2.157

In the second example, a cylinder with the radius $0.1\lambda_0$ and the height $0.25\lambda_0$ ($f_0 = 1$ GHz) was chosen for the comparison of power ratios for the frequencies $f = 0.5$, 0.75, and 1 GHz (all with 3885 tetrahedrons), respectively. It is seen in Figure 4 that the power ratios of real and imaginary parts of total power calculated by the SWG and pulse function methods are near unity for 9, 12, and 15 modes at the frequencies $f = 0.5$, 0.75, and 1 GHz, respectively. The ratio for the imaginary parts of total power does not deviate from unity.

In the last example, a $0.2\lambda_0$ cube with $\varepsilon_r = 4$ and $\varepsilon_r = 9$ was investigated to see the effect of permittivity values on Error($\boldsymbol{J}$), defined in (14). The results are shown in Figure 5. The TEL was chosen as $\lambda_{eff}/10$ for $\varepsilon_r = 9$ and 3894 tetrahedrons was obtained from Altair FEKO®. As seen in Figure 5, Error($\boldsymbol{J}$) is higher than $\varepsilon_r = 4$ in general with the same number of meshes because of higher λ_{eff}. It is observed that increasing the number of meshes up to 10355 tetrahedrons (TEL=$\lambda_{eff}/20$ for $\varepsilon_r = 4$) does not decrease the error because of small contributions from CMs with large eigenvalues (i.e., non-significant modes), which can be seen in Figure 5c. It is believed that further reduction of this error values will be possible by utilizing higher quadrature rules for test functions and careful singularity treatment [8]. The error between $\boldsymbol{J}_{pulse}$ and $\boldsymbol{J}_{SWG}$ was observed to be decreasing when more eigenvalues are used for the calculation of $\boldsymbol{J}$.

4 Conclusion

In this paper, pulse functions and point matching method in VIE are utilized to construct the impedance matrix in the generalized eigenvalue equations, before extracting the CMs. All the tested examples give similar results as obtained for the SWG method using Altair FEKO®. There-

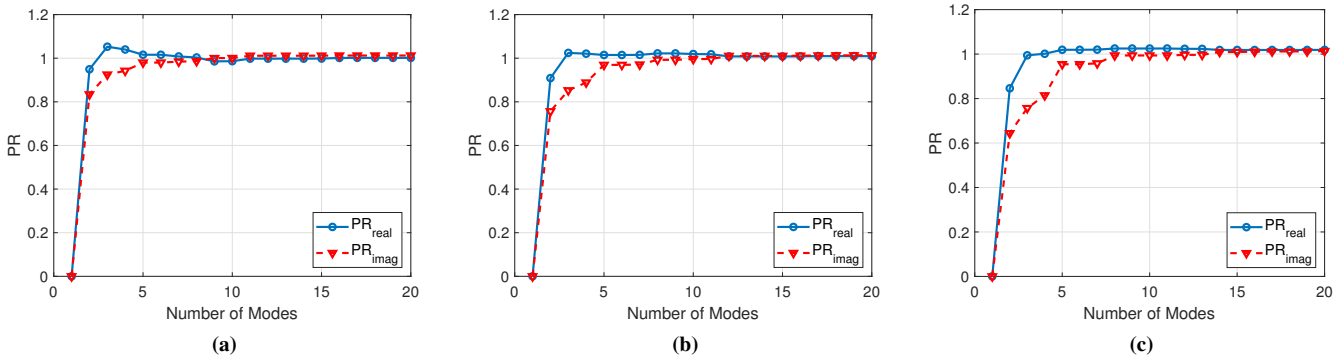

Figure 4. Power ratios of P_{pulse} and P_{SWG} for a scattering problem from a cylinder, $\varepsilon_r = 4$, $r = 0.1\lambda_0$, $h = 0.25\lambda_0$, 3885 tetrahedrons, (a) $f = 0.5$ GHz, (b) $f = 0.75$ MHz, (c) $f = 1$ GHz.

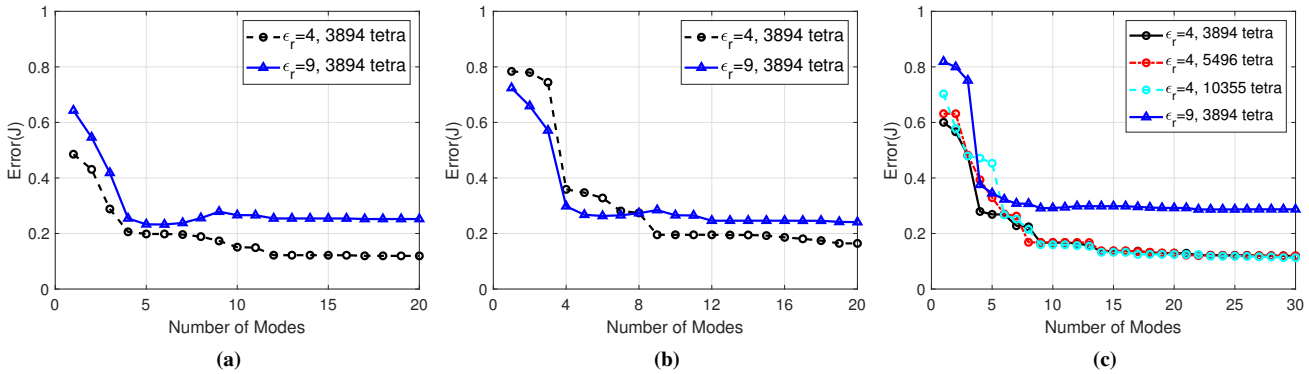

Figure 5. Error between J_{pulse} and J_{SWG}, real part and imaginary parts of J_{pulse} and J_{SWG} involving a scattering problem from a cube, respectively , $\varepsilon_r = 4$ and $\varepsilon_r = 9$, $\ell = 0.2\lambda_0$, (a) $f = 0.5$ GHz, (b) $f = 0.75$ GHz, (c) $f = 1$ GHz.

fore, the proposed method can be considered feasible for CMs extraction of dielectric bodies. In future work, the method will be compared with higher order quadrature methods and different basis functions for dielectric objects.

5 Acknowledgements

We would like to thank Prof. Dr. Adnan Köksal, Prof. Dr. Mats Gustafsson and Dr. Miloslav Capek for their contributions to this paper. The author kindly acknowledges the support from Grant TUBITAK BIDEB 2219 (grant no:1059B191800548).

References

[1] R. J. Garbacz, "Modal Expansions for Resonance Scattering Phenomena," *Proc. IEEE*, 53, 8, Aug. 1965, pp. 856–864.

[2] R. F. Harrington and J. R. Mautz, "Theory of characteristic modes for conducting bodies," *IEEE Trans. Antennas Propag.*, **19**, 5, Sep. 1971, pp. 622–628.

[3] R. F. Harrington, J. R. Mautz, and Y. Chang, "Characteristic Mode for Dielectric and Magnetic Bodies," *IEEE Trans. Antennas Propag.*, **20**, 2, March 1972, pp. 194–198.

[4] Y. Chang and R. F. Harrington, "A surface formulation for characteristic modes of material bodies," *IEEE Trans. Antennas Propag.*, **25**, 6, Nov. 1977, pp. 789–795.

[5] J. Markkanen, and P. Ylä-Oijala, "Discretization of Electric Current Volume Integral Equation with Piecewise Linear Basis Functions," *IEEE Trans. Antennas Propag.*, **62**, 9, Sept. 2014, pp. 4877–4880.

[6] T. K. Sarkar, E. Arvas, and S. Ponnapalli, "Electromagnetic Scattering from Dielectric Bodies," *IEEE Trans. Antennas Propag.*, **37**, 5, May 1989, pp. 673–676.

[7] YY. Zhu, Q. M. Cai, R. Zhang, X. Cao, Y. W. Zhao, B. Gao, and J. Fan, "Discontinuous Galerkin VSIE Method for Electromagnetic Scattering from Composite Metallic and Dielectric Structures," *PIER M.*, **84**, Jan. 2019, pp. 197–209.

[8] M. Capek, V. Losenicky, L. Jelinek, and M. Gustafsson, "Validating the Characteristic Modes Solvers," *IEEE Trans. Antennas Propag.*, **65**, 8, Aug. 2017, pp. 4134–4145.